

Generalized Arcsine Laws for Fractional Brownian Motion

Tridib Sadhu,¹ Mathieu Delorme,² and Kay Jörg Wiese²

¹Tata Institute of Fundamental Research, Mumbai 400005, India

²CNRS-Laboratoire de Physique Théorique de l'Ecole Normale Supérieure, PSL Research University, Sorbonne Universités, UPMC, 24 rue Lhomond, 75005 Paris, France

(Received 7 June 2017; revised manuscript received 9 December 2017; published 26 January 2018)

The three arcsine laws for Brownian motion are a cornerstone of extreme-value statistics. For a Brownian B_t starting from the origin, and evolving during time T , one considers the following three observables: (i) the duration t_+ the process is positive, (ii) the time t_{last} the process last visits the origin, and (iii) the time t_{max} when it achieves its maximum (or minimum). All three observables have the same cumulative probability distribution expressed as an arcsine function, thus the name arcsine laws. We show how these laws change for fractional Brownian motion X_t , a non-Markovian Gaussian process indexed by the Hurst exponent H . It generalizes standard Brownian motion (i.e., $H = \frac{1}{2}$). We obtain the three probabilities using a perturbative expansion in $\epsilon = H - \frac{1}{2}$. While all three probabilities are different, this distinction can only be made at second order in ϵ . Our results are confirmed to high precision by extensive numerical simulations.

DOI: 10.1103/PhysRevLett.120.040603

The three arcsine laws for Brownian motion or more generally for discrete random processes [1–4] are celebrated properties of stochastic processes. For a Brownian B_t starting from the origin, and evolving during time T , one considers the following three observables (see Fig. 1): (i) the total duration t_+ when the process is positive, (ii) the last time t_{last} the process visits the origin, and (iii) the time t_{max} it achieves its maximum (or minimum). Remarkably, all three observables have the same probability distribution as a function of $\vartheta := t/T$,

$$p(\vartheta) = \frac{1}{\pi\sqrt{\vartheta(1-\vartheta)}}. \quad (1)$$

As the cumulative distribution contains an arcsine function, these laws are commonly referred to as the first, second, and third arcsine law. These laws apply quite generally to Markov processes, i.e., processes where the increments are uncorrelated [2]. Their counterintuitive form with a divergence at $\vartheta = 0$ and $\vartheta = 1$ has sparked a lot of interest, and they are considered among the most important properties of stochastic processes. Recent studies led to many extensions, in constrained Brownian motion [5–7], for general stochastic processes [8–13], even in higher dimensions [14–16]. The laws are realized in a plethora of real-world examples, from finance [17,18] to competitive team sports [19].

In this Letter, we ask how these laws change for fractional Brownian motion (FBM) which is a generalization of standard Brownian motion preserving scale invariance as well as translation invariance, both in time and

space. FBM was introduced in its final form by Mandelbrot and Van Ness [20] to describe time-series data in natural processes. It is defined as a Gaussian process X_t , starting at zero, $X_0 = 0$, with mean $\langle X_t \rangle = 0$ and covariance

$$\langle X_t X_s \rangle = t^{2H} + s^{2H} - |t-s|^{2H}. \quad (2)$$

The parameter $H \in (0, 1)$ is the Hurst exponent. Standard Brownian motion corresponds to $H = \frac{1}{2}$ where the covariance reduces to $\langle X_t X_s \rangle = 2 \min(s, t)$. Unless $H = \frac{1}{2}$, the process is non-Markovian; i.e., its increments are not independent.

For $H > \frac{1}{2}$ they are positively correlated, while for $H < \frac{1}{2}$ they are anticorrelated. This non-Markovian nature makes a theoretical analysis of FBM difficult, and only a few exact

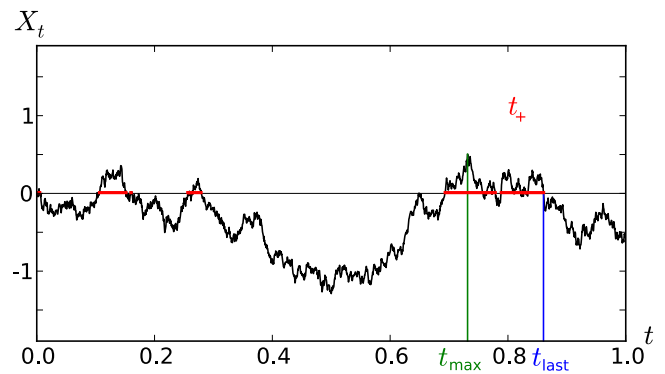


FIG. 1. The three observables t_+ , t_{last} , and t_{max} considered in this Letter.

results are available in the literature [21–23], in particular, for functionals of the trajectories [24–26].

FBM is important as it successfully models a variety of natural processes [27]: a tagged particle in the single file ($H = 0.25$) [28,29], the integrated current in diffusive transport ($H = 0.25$) [30], polymer translocation through a narrow pore ($H \approx 0.4$) [31–33], anomalous diffusion [34,35], values of the log return of a stock ($H \approx 0.6$ to 0.8) [36–39], hydrology ($H \approx 0.72$ to 0.87) [40], a tagged monomer in a polymer ($H = 0.25$) [41], solar flare activity ($H \approx 0.57$ to 0.86) [42], the price of electricity in a liberated market ($H \approx 0.41$) [43], telecommunication networks ($H \approx 0.78$ to 0.86) [44], telomeres inside the nucleus of human cells ($H \approx 0.18$ to 0.35) [45], or diffusion inside crowded fluids ($H \approx 0.4$) [46]. Generalizing the three arcsine laws (1) to FBM thus has fundamental importance, as well as a multitude of potential applications.

Unlike for Brownian motion, the probabilities of the three observables t_+ , t_{last} , and t_{max} are different. Using an expansion in $\epsilon = H - \frac{1}{2}$, we derive them in the form

$$p_+(\vartheta) = \frac{\mathcal{N}_+}{[\vartheta(1-\vartheta)]^H} e^{\epsilon \mathcal{F}_1^+(\vartheta) + \epsilon^2 \mathcal{F}_2^+(\vartheta) + \mathcal{O}(\epsilon^3)}, \quad (3)$$

$$p_{\text{last}}(\vartheta) = \frac{\mathcal{N}_{\text{last}}}{\vartheta^H(1-\vartheta)^{1-H}} e^{\epsilon \mathcal{F}_1^{\text{last}}(\vartheta) + \epsilon^2 \mathcal{F}_2^{\text{last}}(\vartheta) + \mathcal{O}(\epsilon^3)}, \quad (4)$$

$$p_{\text{max}}(\vartheta) = \frac{\mathcal{N}_{\text{max}}}{[\vartheta(1-\vartheta)]^H} e^{\epsilon \mathcal{F}_1^{\text{max}}(\vartheta) + \epsilon^2 \mathcal{F}_2^{\text{max}}(\vartheta) + \mathcal{O}(\epsilon^3)}. \quad (5)$$

The prefactors of the exponential are predicted using scaling arguments for $\vartheta \rightarrow 0$ and $\vartheta \rightarrow 1$. They are linked to the persistence exponent $\theta = 1 - H$ [21,22]. For example, Eq. (4) is approximately the probability to return to the origin $\sim \vartheta^{-H}$ and never to return afterwards $\sim (1-\vartheta)^{-\theta}$. The terms in the exponential are nontrivial and remain finite over the full range of ϑ . We use the convention that the integral over each \mathcal{F} function vanishes, which adjusts the normalization constants \mathcal{N} . To leading order we find

$$\begin{aligned} \mathcal{F}_1^+(\vartheta) &= \mathcal{F}_1^{\text{max}}(\vartheta) \\ &= \pi \sqrt{\frac{1-\vartheta}{\vartheta}} + \frac{2(2\vartheta-1)\text{acos}(\sqrt{\vartheta})}{\sqrt{(1-\vartheta)\vartheta}} - \frac{\pi^2}{2} + 2, \end{aligned} \quad (6)$$

$$\mathcal{F}_1^{\text{last}}(\vartheta) = 0. \quad (7)$$

The expression of $\mathcal{F}_1^{\text{max}}(\vartheta)$ was reported earlier [47–50]. The equality of \mathcal{F}_1^+ and $\mathcal{F}_1^{\text{max}}$, and their difference from the vanishing $\mathcal{F}_1^{\text{last}}$, is qualitatively seen in Fig. 2. We have no intuitive understanding of this coincidence.

A numerical estimation of the three probabilities is obtained using a discrete-time algorithm [51] for FBM of a given H , which generates sample trajectories drawn from a Gaussian probability with covariance (2). The

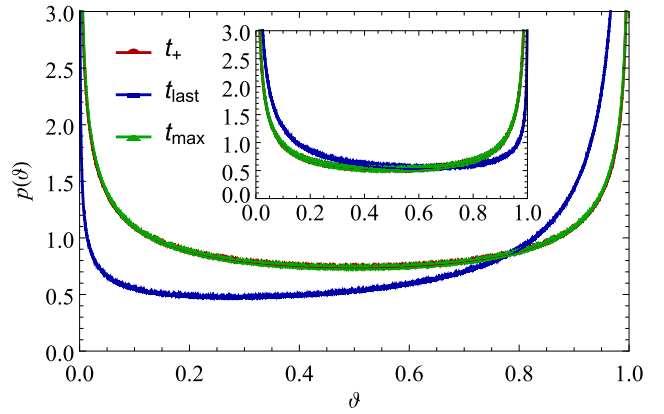


FIG. 2. Numerical simulation results for the probability of the three observables t_{last} , t_+ , and t_{max} for a FBM with $H = 0.33$. The inset shows the probabilities for $H = 0.66$. Note that the distributions of t_+ and t_{max} are almost indistinguishable.

probabilities in Figs. 2 and 3 are obtained by averaging over 5×10^9 sample trajectories, each with 2^{13} time steps.

Figure 2 shows that $p_{\text{last}}(\vartheta)$ behaves markedly differently from the other two distributions; especially, it is asymmetric under the exchange $\vartheta \rightarrow 1 - \vartheta$. This can be seen in the scaling part of Eq. (4), where the exponent H comes from the return probability to the starting point, while the survival exponent $\theta = 1 - H$ governs the divergence for $\vartheta \rightarrow 1$. This asymmetry in exponents is reversed around $H = \frac{1}{2}$, as seen in the inset of Fig. 2.

The analytical expressions for \mathcal{F}_2 in Eqs. (3)–(5) are cumbersome; we will sketch the derivation for the simplest one, $\mathcal{F}_2^{\text{last}}(\vartheta)$, below, while the remaining ones will be reported elsewhere [52].

Confirmation of our theoretical results comes from comparison with numerical simulations of the probabilities presented in Fig. 3 for $\epsilon = -0.17$. Deviations start becoming visible for $|\epsilon| \approx 0.25$ and higher (see Supplemental

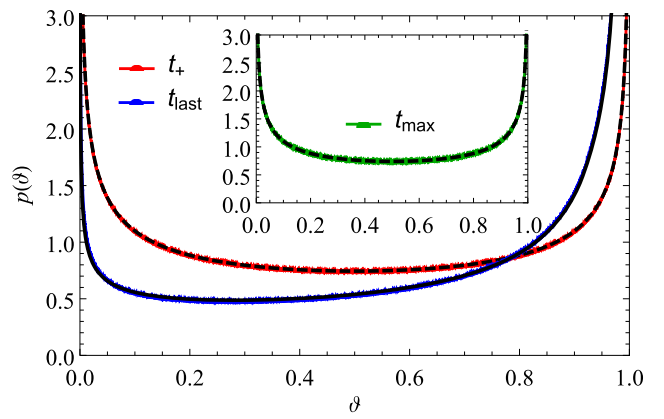


FIG. 3. Comparison of the formulas (3)–(5) with their corresponding numerical simulation result of a FBM with $H = 0.33$. The dashed lines are the theoretical result. $p_{\text{max}}(\vartheta)$ is shown in the inset as it is almost indistinguishable from $p_+(\vartheta)$.

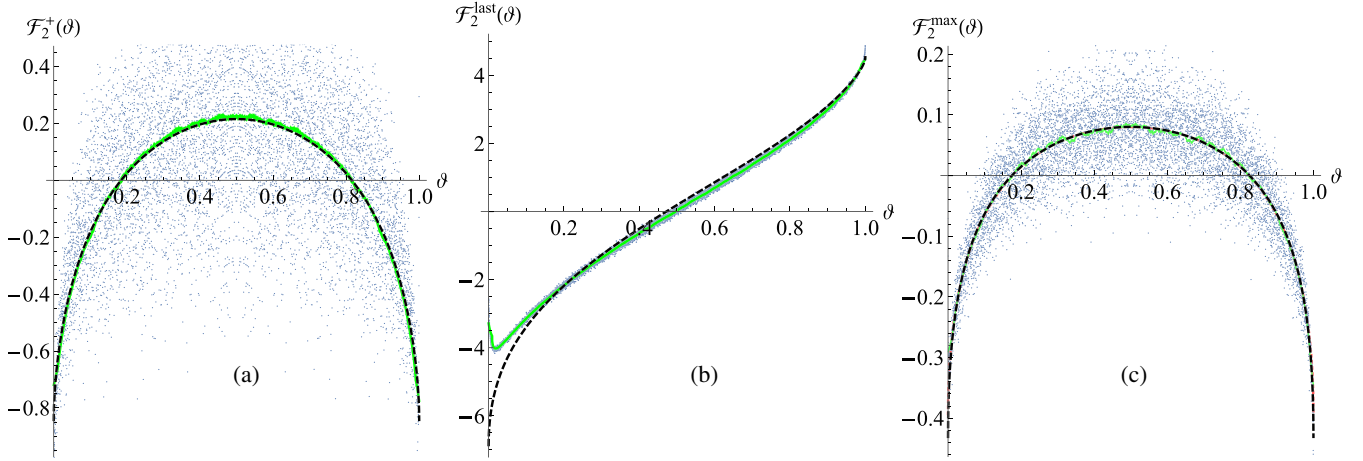


FIG. 4. A comparison for the three $\mathcal{F}_2(\theta)$ obtained analytically (black dashed lines) and their measurement using formula (9) with $\varepsilon = \pm \frac{1}{6}$. From left to right: (a) positive time, (b) time of the last visit to the origin, and (c) time for the maximum. The scattered dots are the raw data from trajectories of $N = 2^{13}$ time steps, averaged over 5×10^9 samples, which are coarse grained by a factor of 100 to give the green curve. Approximations of our analytical results are given in the Supplemental Material [53].

Material [53]). For a finer comparison we plot our theoretical results of $\mathcal{F}_2(\theta)$ in Fig. 4 alongside their extraction from numerical simulations. To illustrate our procedure, we use Eq. (3) to define

$$\mathcal{F}_{2,\varepsilon}^+(\theta) := \frac{1}{\varepsilon} \left[\frac{1}{\varepsilon} \ln \left(p_+(\theta) \frac{[\theta(1-\theta)]^H}{\mathcal{N}^+} \right) - \mathcal{F}_1^+(\theta) \right]. \quad (8)$$

Then, $\mathcal{F}_{2,\varepsilon}^+(\theta) = \mathcal{F}_2^+(\theta) + \mathcal{O}(\varepsilon)$ which contains all terms in the exponential in Eq. (3) except $\mathcal{F}_1^+(\theta)$. One can improve this estimation by using that the subleading term in $\mathcal{F}_{2,\varepsilon}^+(\theta)$ is odd in ε , to define

$$\bar{\mathcal{F}}_{2,\varepsilon}^+(\theta) := \frac{1}{2} [\mathcal{F}_{2,\varepsilon}^+(\theta) + \mathcal{F}_{2,-\varepsilon}^+(\theta)] = \mathcal{F}_2^+(\theta) + \mathcal{O}(\varepsilon^2). \quad (9)$$

A comparison of $\bar{\mathcal{F}}_{2,\varepsilon}^+(\theta)$ extracted from numerical simulations of $p_+(\theta)$ with the theoretical result of $\mathcal{F}_2^+(\theta)$ is plotted in Fig. 4 for $\varepsilon = \pm \frac{1}{6}$. The figure also contains the comparison for $\mathcal{F}_2^{\text{last}}(\theta)$ and $\mathcal{F}_2^{\text{max}}(\theta)$. As one sees, the agreement between theory and numerical simulations is quite striking: we remind the reader that these are sub-subleading corrections, almost indiscernable in Fig. 3. We note the much larger amplitude of $\mathcal{F}_2^{\text{last}}(\theta)$. The latter also has the largest deviations from the theory, especially for $\theta \rightarrow 0$. These deviations indicate the presence of subleading terms of order ε^4 , or higher.

In Fig. 2 the probabilities $p_+(\theta)$ and $p_{\text{max}}(\theta)$ are difficult to distinguish from each other. Their difference can analytically be seen only at second order in ε . To underline that these are distinct distributions, we show the difference $\delta\mathcal{F}_2(\theta) = \mathcal{F}_2^{\text{max}}(\theta) - \mathcal{F}_2^+(\theta)$ in Fig. 5.

In the rest of this Letter we sketch the derivation of formulas (3)–(5). We begin with the action which characterizes the probability of a FBM trajectory,

$$\mathcal{S}[X] = \int_0^T dt_1 \int_{t_1}^T dt_2 \dot{X}_{t_1} \mathcal{C}^{-1}(t_1, t_2) \dot{X}_{t_2}. \quad (10)$$

Here $\mathcal{C}(t_1, t_2)$ is the covariance given in Eq. (2). We use an expansion [48,54] of the action around $H = \frac{1}{2}$ to take advantage of the Markov property of Brownian motion. One writes

$$\begin{aligned} & \mathcal{C}(t_1, t_2) \\ &= 2D_\varepsilon \left(\delta(t_1 - t_2) + \frac{\varepsilon}{|t_1 - t_2|} + \frac{2\varepsilon^2 \ln |\frac{t_1 - t_2}{\tau}|}{|t_1 - t_2|} + \mathcal{O}(\varepsilon^3) \right) \end{aligned} \quad (11)$$

which leads to an expansion of the action [55]

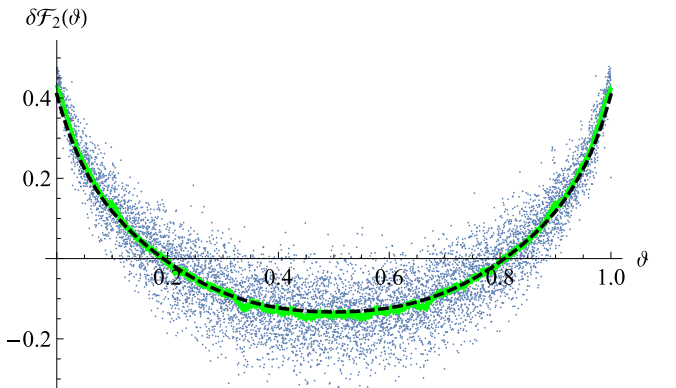


FIG. 5. The difference $\delta\mathcal{F}_2(\theta) = \mathcal{F}_2^{\text{max}}(\theta) - \mathcal{F}_2^+(\theta)$, using the same conventions as in Fig. 4. This plot quantifies the difference between the first and third arcsine law.

$$S[X] = \frac{1}{2D_\epsilon} \int_0^T dt_1 \int_{t_1}^T dt_2 \dot{X}_{t_1} \dot{X}_{t_2} \left[\delta(t_1 - t_2) + \frac{\epsilon}{|t_1 - t_2|} + \int_{t_1}^{t_2} ds \frac{\epsilon^2}{|t_1 - s||t_2 - s|} + \mathcal{O}(\epsilon^3) \right] \quad (12)$$

where $D_\epsilon \simeq (1 + 2\epsilon)\tau^{2\epsilon}$ and all expressions are regularized by an ultraviolet cutoff τ in time.

Our calculation for the probabilities is done in Laplace variables. One reason for this choice is that the space integrals appearing in perturbation theory are easier. A further advantage is that temporal convolutions become mere products in the conjugate Laplace variables. The action (12) is expressed in Laplace variables by writing

$$\frac{\Theta(|t_1 - t_2| - \tau)}{|t_1 - t_2|} \simeq \int_0^\Lambda dy e^{-y|t_1 - t_2|}. \quad (13)$$

Here Λ is a UV cutoff related to the cutoff τ in time via [48] $\Lambda = (1/\tau)e^{-\gamma_E}$ where γ_E is Euler's constant. As an explicit example, let us consider the calculation of $P_{\text{last}}(t, T)$ and its Laplace transform

$$\tilde{P}_{\text{last}}(\lambda, s) = \int_0^\infty dT \int_0^T dt e^{-\lambda t - sT} P_{\text{last}}(t, T). \quad (14)$$

The quantity of interest $P_{\text{last}}(t, T)$ has a scaling form $P_{\text{last}}(t, T) = T p_{\text{last}}(t/T)$ which using Eq. (14) yields

$$\tilde{P}_{\text{last}}(\lambda, s) = \frac{1}{s} \int_0^1 d\theta \frac{p_{\text{last}}(\theta)}{1 + \kappa\theta}; \quad \kappa = \frac{\lambda}{s}. \quad (15)$$

Defining $\tilde{p}_{\text{last}}(\kappa) := s\tilde{P}_{\text{last}}(\lambda, s)$, one obtains the probability $p_{\text{last}}(\theta)$ by taking the inverse transformation

$$p_{\text{last}}(\theta) = \lim_{\phi \rightarrow \pi} \frac{-1}{\pi i \theta} \Im \tilde{p}_{\text{last}}(\kappa = e^{i\phi}/\theta), \quad (16)$$

where \Im denotes the imaginary part. This is proven from Eq. (15) using the Sokhotski-Plemelj-Weierstrass theorem [56,57] in complex analysis.

The calculation is simplest at order zero in ϵ , i.e., for a Brownian. Using Eqs. (12) and (14) one writes

$$\tilde{P}_{\text{last}}^{H=\frac{1}{2}}(\lambda, s) = \lim_{x_0 \rightarrow 0} \frac{2}{x_0} \int_0^\infty dx \tilde{Z}(x_0, x_0, s + \lambda) \tilde{Z}^+(x_0, x, s). \quad (17)$$

Here $\tilde{Z}(x, y, s) = (2\sqrt{s})^{-1} \exp(-\sqrt{s}|x - y|)$ is the Laplace transform of the Brownian propagator, while $\tilde{Z}^+(x, y, s) = Z(x, y, s) - Z(x, -y, s)$ is the propagator in presence of an absorbing wall at the origin. This yields

$$\tilde{p}_{\text{last}}^{H=\frac{1}{2}}(\kappa) = s\tilde{P}_{\text{last}}^{H=\frac{1}{2}}(s\kappa, s) = \frac{1}{\sqrt{1 + \kappa}}. \quad (18)$$

Using the transform (16) one obtains the arcsine law (1).

Perturbative corrections to the probability are evaluated by following a similar procedure [48]. Contributions at different orders in ϵ are represented by the diagrams in Fig. 6. The nonvanishing contributions at order ϵ come from the two diagrams (a) and (b) which like (17) are expressed in terms of the Brownian propagator. For example, the amplitude corresponding to diagram (a) is

$$\frac{4\epsilon}{x_0} \int_0^\Lambda dy \int_{-\infty}^\infty dx_1 \int_{-\infty}^\infty dx_2 \int_0^\infty dx \tilde{Z}(x_0, x_1, s_1) \\ \times \partial_{x_1} \tilde{Z}(x_1, x_2, s_1 + y) \partial_{x_2} \tilde{Z}(x_2, x_0, s_1) \tilde{Z}^+(x_0, x, s) \quad (19)$$

where $s_1 = s(1 + \kappa)$. This leads to the nontrivial power law in Eq. (4) and a vanishing $\mathcal{F}_1^{\text{last}}$ in Eq. (7).

At order ϵ^2 , there are multiple diagrams which contribute to the probability $\tilde{p}_{\text{last}}(\theta)$. However, the only contributions to $\mathcal{F}_2^{\text{last}}$ come from the two diagrams (c) and (d) in Fig. 6. After some tedious algebra, the net amplitude of the two diagrams reads

$$\tilde{\mathcal{F}}_2^{\text{last}}(\kappa) = - \int_0^\Lambda dy_1 dy_2 [\sqrt{\kappa + y_1 + y_2 + 1} - \sqrt{\kappa + y_1 + 1} \\ - \sqrt{\kappa + y_2 + 1} + \sqrt{\kappa + 1}] \times \frac{2\sqrt{1 + \kappa} \sqrt{y_1 + y_2 + 1}}{y_1^2 y_2^2} \\ \times (1 - \sqrt{y_1 + 1} - \sqrt{y_2 + 1} + \sqrt{y_1 + y_2 + 1}). \quad (20)$$

Finally, $\mathcal{F}_2^{\text{last}}(\theta)$ is obtained using

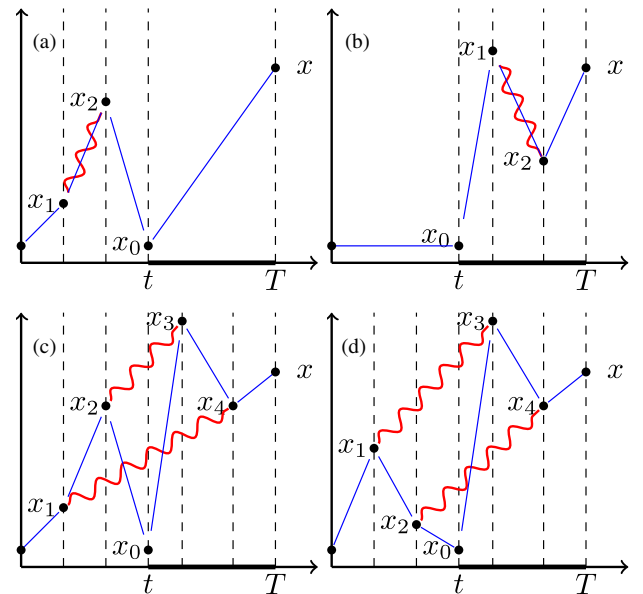


FIG. 6. The diagrams (a) and (b) contributing to the order- ϵ term in $p_{\text{last}}(\theta)$, as well as (c) and (d) contributing to the order- ϵ^2 term $\mathcal{F}_2^{\text{last}}(\theta)$ in (4). Solid lines denote the Brownian propagators, with absorbing boundary conditions indicated by a bold line after time t . The curly lines represent the order- ϵ interaction in Eq. (12).

$$\mathcal{F}_2^{\text{last}}(\vartheta) = \lim_{\phi \rightarrow \pi} \Re \tilde{\mathcal{F}}_2^{\text{last}}(\kappa = e^{i\phi}/\vartheta), \quad (21)$$

which follows from Eqs. (16) and (4) [58]. Integrals in Eq. (20) converge for $\Lambda \rightarrow \infty$ leading to the result shown in the middle of Fig. 4.

Similar calculations for the other two probabilities $P_+(\vartheta)$ and $P_{\max}(\vartheta)$ are more involved. For example, in $p_{\max}(\vartheta)$ ten diagrams contribute to the power law $[\vartheta(1 - \vartheta)]^{-H}$ in Eq. (5); in addition there are seven diagrams which contribute to \mathcal{F}_2^{\max} . All these terms need to be grouped with the appropriate repeated first-order diagrams to yield combinations which converge for $\Lambda \rightarrow \infty$. These calculations will be reported elsewhere [52].

To summarize, we calculated the probabilities (3)–(5) generalizing the three arcsine laws to FBM up to order ε^2 , improved by incorporating the exact scaling results for $\vartheta \rightarrow 0$ and 1. Our numerical simulations confirm these highly nontrivial predictions accurately.

Most realizations of FBM found in practical applications fall within the range $H = \frac{1}{2} \pm 0.25$ where our formulas yield high-precision predictions. Our approach further offers a systematic framework to obtain other analytical results for non-Markovian processes, of which very few are available so far.

We thank J. Klamser, P. Krapivsky, S. N. Majumdar, and A. Rosso for stimulating discussions, and PSL for support by Grant No. ANR-10-IDEX-0001-02-PSL. This research was supported in part by ICTS-TIFR (Code: ICTS/Prog-NESP/2015/10).

- [9] G. Schehr and P. le Doussal, Extreme value statistics from the real space renormalization group: Brownian motion, Bessel processes and continuous time random walks, *J. Stat. Mech.* (2010) P01009.
- [10] K. J. Hochberg and E. Orsingher, The arcsine law and its analogs for processes governed by signed and complex measures, *Stoch. Proc. Appl.* **52**, 273 (1994).
- [11] J. Pitman and M. Yor, Arcsine laws and interval partitions derived from a stable subordinator, *Proc. London Math. Soc.* **65**, 326 (1992).
- [12] P. Carmona, F. Petit, and M. Yor, Some extensions of the arcsine law as partial consequences of the scaling property of Brownian motion, *Probab. Theory Relat. Fields* **100**, 1 (1994).
- [13] J. Lamperti, An occupation time theorem for a class of stochastic processes, *Trans. Am. Math. Soc.* **88**, 380 (1958).
- [14] M. Barlow, J. Pitman, and M. Yor, in *Siminaire de Probabilités XXIII* (Springer, Berlin, 1989), pp. 294–314.
- [15] N. H. Bingham and R. A. Doney, On higher-dimensional analogues of the arcsine law, *J. Appl. Probab.* **25**, 120 (1988).
- [16] P. A. Ernst and L. Shepp, On occupation times of the first and third quadrants for planar Brownian motion, *J. Appl. Probab.* **54**, 337 (2017).
- [17] C. Dale and R. Workman, The arcsine law and the treasury bill futures market, *Financ. Anal. J.* **36**, 71 (1980).
- [18] J. Baz and G. Chacko, *Financial Derivatives: Pricing, Applications, and Mathematics* (Cambridge University Press, Cambridge, England, 2004).
- [19] A. Clauset, M. Kogan, and S. Redner, Safe leads and lead changes in competitive team sports, *Phys. Rev. E* **91**, 062815 (2015).
- [20] B. B. Mandelbrot and J. W. Van Ness, Fractional Brownian motions, fractional noises and applications, *SIAM Rev.* **10**, 422 (1968).
- [21] G. M. Molchan, Maximum of a fractional Brownian motion: Probabilities of small values, *Commun. Math. Phys.* **205**, 97 (1999).
- [22] J. Krug, H. Kallabis, S. N. Majumdar, S. J. Cornell, A. J. Bray, and C. Sire, Persistence exponents for fluctuating interfaces, *Phys. Rev. E* **56**, 2702 (1997).
- [23] T. Guérin, N. Levernier, O. Bénichou, and R. Voituriez, Mean first-passage times of non-Markovian random walkers in confinement, *Nature (London)* **534**, 356 (2016).
- [24] M. Schwarzl, A. Godec, and R. Metzler, Quantifying nonergodicity of anomalous diffusion with higher order moments *Sci. Rep.* **7**, 3878 (2017).
- [25] T. Verechaguina, I. M. Sokolov, and L. Schimansky-Geier, First passage time densities in non-Markovian models with subthreshold oscillations, *Europhys. Lett.* **73**, 691 (2006).
- [26] G. Molchan and A. Khokhlov, Small values of the maximum for the integral of fractional Brownian motion, *J. Stat. Phys.*, **114**, 923 (2004).
- [27] L. Decreusefond and A. S. Üstünel, Fractional Brownian motion: Theory and applications, in *ESAIM: PROC*, 1998, pp. 75–86, <http://citeseerx.ist.psu.edu/viewdoc/summary?doi=10.1.1.28.1848>.
- [28] P. L. Krapivsky, K. Mallick, and T. Sadhu, Dynamical properties of single-file diffusion, *J. Stat. Mech.* (2015) P09007.

- [29] T. Sadhu and B. Derrida, Large deviation function of a tracer position in single-file diffusion, *J. Stat. Mech.* (2015) P09008.
- [30] T. Sadhu and B. Derrida, Correlations of the density and of the current in non-equilibrium diffusive systems, *J. Stat. Mech.* (2016) 113202 (2016).
- [31] A. Zoia, A. Rosso, and S. N. Majumdar, Asymptotic Behavior of Self-Affine Processes in Semi-Infinite Domains, *Phys. Rev. Lett.* **102**, 120602 (2009).
- [32] J. L. A. Dubbeldam, V. G. Rostiashvili, A. Milchev, and T. A. Vilgis, Fractional Brownian motion approach to polymer translocation: The governing equation of motion, *Phys. Rev. E* **83**, 011802 (2011).
- [33] V. Palyulin, T. Ala-Nissila, and R. Metzler, Polymer translocation: The first two decades and the recent diversification, *Soft Matter* **10**, 9016 (2014).
- [34] J.-P. Bouchaud and A. Georges, Anomalous diffusion in disordered media: Statistical mechanisms, models and physical applications, *Phys. Rep.* **195**, 127 (1990).
- [35] R. Metzler and J. Klafter, The random walk's guide to anomalous diffusion: A fractional dynamics approach, *Phys. Rep.* **339**, 1 (2000).
- [36] E. E. Peters, *Chaos and Order in the Capital Markets*, 2nd ed., Wiley Finance Editions (Wiley, New York, 1996).
- [37] N. J. Cutland, P. E. Kopp, and W. Willinger, in *Seminar on Stochastic Analysis, Random Fields and Applications, Progress in Probability* edited by E. Bolthausen, M. Dozzi, and F. Russo (Birkhäuser, Basel, 1995), Vol. 36, pp. 327–351.
- [38] F. Biagini, Y. Hu, B. Oksendal, and T. Zhang, *Stochastic Calculus for Fractional Brownian Motion and Applications* (Springer Verlag, London, 2008).
- [39] T. Sottinen, Fractional Brownian motion, random walks and binary market models, *Finance Stochastics* **5**, 343 (2001).
- [40] B. B. Mandelbrot and J. R. Wallis, Noah, Joseph, and operational hydrology, *Water Resour. Res.* **4**, 909 (1968).
- [41] S. Gupta, A. Rosso, and C. Texier, Dynamics of a Tagged Monomer: Effects of Elastic Pinning and Harmonic Absorption, *Phys. Rev. Lett.* **111**, 210601 (2013).
- [42] E. Monte-Moreno and M. Hernández-Pajares, Occurrence of solar flares viewed with GPS: Statistics and fractal nature, *J. Geophys. Res.* **119**, 9216 (2014).
- [43] I. Simonsen, Measuring anti-correlations in the nordic electricity spot market by wavelets, *Physica A (Amsterdam)* **322**, 597 (2003).
- [44] I. Norros, On the use of fractional Brownian motion in the theory of connectionless networks, *IEEE J. Sel. Areas Commun.* **13**, 953 (2006).
- [45] K. Burnecki, E. Kepten, J. Janczura, I. Bronshtein, Y. Garini, and A. Weron, Universal algorithm for identification of fractional Brownian motion. A case of telomere sub-diffusion, *Biophys. J.* **103**, 1839 (2012).
- [46] D. Ernst, M. Hellmann, K. Jürgen, and M. Weiss, Fractional Brownian motion in crowded fluids, *Soft Matter* **8**, 4886 (2012).
- [47] M. Delorme and K. J. Wiese, The Maximum of a Fractional Brownian Motion: Analytic Results from Perturbation Theory, *Phys. Rev. Lett.* **115**, 210601 (2015).
- [48] M. Delorme and K. J. Wiese, Perturbative expansion for the maximum of fractional Brownian motion, *Phys. Rev. E* **94**, 012134 (2016).
- [49] M. Delorme and K. J. Wiese, Extreme-value statistics of fractional Brownian motion bridges, *Phys. Rev. E* **94**, 052105 (2016).
- [50] M. Delorme, Ph.D. thesis, PSL Research University, 2016.
- [51] A. B. Dieker, Master's thesis, Vrije Universiteit, Amsterdam, 2002.
- [52] T. Sadhu and K. J. Wiese, Statistics of certain functionals of fractional Brownian motion (to be published).
- [53] See Supplemental Material at <http://link.aps.org/supplemental/10.1103/PhysRevLett.120.040603> for comparison of theoretical results with numerical simulation at multiple values of H .
- [54] K. J. Wiese, S. N. Majumdar, and A. Rosso, Perturbation theory for fractional Brownian motion in presence of absorbing boundaries, *Phys. Rev. E* **83**, 061141 (2011).
- [55] The action is written in a form that when evaluating it in perturbation theory, so-called “contact terms” proportional to δ functions in time from the contraction of two \dot{X} have to be discarded.
- [56] A. D. Polyanin and A. V. Manzhirov, *Handbook of Integral Equations* (Taylor & Francis, New York, 1998).
- [57] N. I. Muskhelishvili and J. R. M. Radok, *Singular Integral Equations: Boundary Problems of Function Theory and Their Application to Mathematical Physics* (Dover Publications, New York, 2008).
- [58] It contains the real part \Re , as it is divided by the order-0 result (18).